analytical chemistry

Article

Cite This: Anal. Chem. 2018, 90, 4719−4724

pubs.acs.org/ac

Au−Se-Bond-Based Nanoprobe for Imaging MMP-2 in Tumor Cells under a High-Thiol Environment

Xiaonan Gao,[†] Lulu Jiang,[†] Bo Hu, Fanpeng Kong, Xiaojun Liu, Kehua Xu,* and Bo Tang*

College of Chemistry, Chemical Engineering and Materials Science, Collaborative Innovation Center of Functionalized Probes for Chemical Imaging in Universities of Shandong, Key Laboratory of Molecular and Nano Probes, Ministry of Education, Shandong Provincial Key Laboratory of Clean Production of Fine Chemicals, Shandong Normal University, Jinan 250014, P. R. China

Supporting Information

ABSTRACT: The gold nanosensors based on the Au−S bond have been widely applied to biochemical detections. However, signal distortion caused by biothiols has been seldom mentioned and urgently needs to be solved. Herein, we designed a novel but easily assembled gold nanoprobe by coupling a selenol-modified peptide with FITC onto the gold nanoparticle's surface via an Au−Se bond for fluorescence imaging of a tumor marker matrix, metalloproteinases 2 (MMP-2). Compared to the Au−S probes, the Au−Se probes display high thermal stability and a very good anti-interference ability toward glutathione under simulated physiological conditions. More importantly, the Au−Se nanoprobe exhibits a high-fidelity fluorescent signal toward MMP-2, effectively avoiding interference caused by high levels of thiol compounds in vivo. In addition, in vivo experiments further proved that no significant signal intensity change for the tumor cells treated by the Au−Se probes was observed before and after eliminating glutathione. Hence, we believe such Au−Se probes with in vivo glutathione interfering resistance offer new routes and perspectives in biology and medicine in the future.

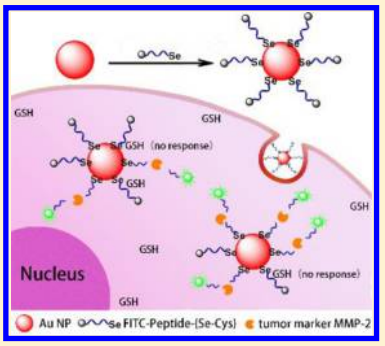

Gold nanoparticle (Au NP) biosensors assembled via an Au−S covalent bond for biomolecule imaging have now been extensively investigated[1−4] due to their decent biocompatibility,[5] low toxicity,[6] and unique tunable optical properties.[7] Such nanobiotechnology of the Au NPs was first developed by Storhoff's group[8] and Schultz's group[9] for assembling DNA onto Au NPs via an Au−S bond. Thereafter, numerous nanomaterials and biomaterials, including DNA, RNA, peptides, and other molecules, have been reported to be assembled onto the Au NPs for bioimaging and molecular detection.[10−15] However, the process of applying the Au NP biosensors in biological systems is still a great challenge, because thiol-functionalized Au NPs process a competitive ligand exchange due to abundant in vivo thiols like glutathione (GSH),[16] resulting in detection signal distortions and rising false positives[17] in tumor diagnosis.

To address the problem, a lot of effort has been done through different outlooks. For instance, Wang's group[18] presented an indirect calibration method that utilizes two fluorophore-labeled "flares" to measure intracellular mRNA for avoiding the false positive result. In 2015, our group had reported a multicolor fluorescence nanoprobe for simultaneous monitoring of multiple tumor markers. Two mRNAs, MMP-2, and MMP-7 were detected by the Au NPs assembled with molecular beacons and peptides, effectively eliminating the false positive signals of the single marker.[19] In fact, the multicolor nanoprobe still suffers from the problem of a high in vitro and in vivo concentration of GSH. Recently, our team has found that selenol can rapidly break Au−S bonds by forming more stable Au−Se bonds, leading to a novel imaging method for selenol in living cells and in vivo.[20,21] Therefore, due to the similar physical and chemical properties of Se and S as well as the high stability of Au−Se bond,[22−24] we anticipate a new Au NPs nanosensor by replacing Au−S with Au−Se bonds, which will solve the interference problem from biothiols.

In this regard, a novel nanoprobe (Au−Se probe) for the detection and imaging of matrix metalloproteinases 2[25] (MMP-2) was designed and synthesized. Since the up regulation of MMPs is closely related to the metastasis of cancer,[26−28] MMP-2 has been considered as a significant biomarker for early cancer diagnosis and a target for therapeutic drug development,[25,29−33] especially in liver cancer,[34,35] breast cancer,[36] and cervical cancer.[37,38] The peptide Gly−Pro−Leu−Gly−Val−Arg−Gly[39] can be specifically cleaved by MMP-2, recovering the fluorophore's fluorescence that was previously quenched by the Au NPs. Interestingly, the Au−Se probe has a superior stability against GSH (high concentration) interferences, leading to a sensitive detection signal for MMP-2 with a high signal-to-noise ratio (SNR, 10.1) and a low limit of detection (LOD, 1.7 ng/mL) under simulated physiological conditions. Especially in comparison with thiol-modified peptide chains of the Au−S probe, which has an SNR of 3.9 and an LOD of 3.1 ng/mL, the Au−Se probe is proved to be a better candidate for detection. The Au−Se probe possesses an excellent stability in biological systems and could provide real information on target molecules.

Received: December 20, 2017
Accepted: March 9, 2018
Published: March 9, 2018

DOI: 10.1021/acs.analchem.7b05343
Anal. Chem. 2018, 90, 4719−4724

EXPERIMENTAL SECTION

Materials. MMP-2 was purchased from ProSpec. MMP activator *p*-aminophenyl mercuric acid was purchased from Genmed Scientifics, U.S.A. MMP was activated by incubation with 1.0 mM of *p*-aminophenyl mercuric for 1 h at 37 °C prior to use. Sodium dodecyl sulfate, Brij 35, sodium chloride, calcium chloride, hydrogen tetrachloroaurate ($HAuCl_4 \cdot 4H_2O$), mercaptoethanol, Tris (2-carboxyethyl) phosphine hydrochloride, trisodium citrate ($C_6H_5Na_3O_7 \cdot 2H_2O$), and phosphate buffer saline (PBS) were purchased from China National Pharmaceutical (Shanghai, China). 3-(4,5-Dimethylthiazol-2-yl)-2,5-diphenyltetrazolium bromide (MTT), *N*-ethylmaleimide, GSH DAPI, cysteine, and selenocystine were purchased from Sigma. All of the chemicals were of analytical grade and used without further purification. Sartorius ultrapure water (18.2 MΩ·cm^2) was used throughout the experiments.

The FITC-modified peptide chains (FITC−Acp−Gly−Pro−Leu−Gly−Val−Arg−Gly−Cys and FITC−Acp−Gly−Pro−Leu−Gly−Val−Arg−Gly−{Se−Cys}) were synthesized and purified by Kangbei (Ningbo, China), and the mass spectrum and high-performance liquid chromatography are shown in the Supporting Information (Figures S1−S4).

Cell culture products, unless mentioned otherwise, were purchased from GIBCO. Human hepatocellular liver carcinoma cell line HepG2 and human hepatocyte cell line HL-7702 were obtained from the Committee on Type Culture Collection of the Chinese Academy of Sciences. The human breast cancer cell line MCF-7 was purchased from KeyGEN biotechnology Company (Nanjing, China).

Instruments. All pH values were measured by a pH-3c digital pH meter (LeiCi, China) with a combined glass-calomel electrode. UV−vis absorption spectra were measured on a Pharmaspec UV-1700 UV−visible spectrophotometer (Shimadzu, Japan). Transmission electron microscopy (TEM) was carried out on a JEM-2100 electron microscope, and the samples were prepared via carbon-coated copper grids. Fluorescence spectra were obtained through an FLS-920 Edinburgh Fluorescence Spectrometer with a xenon lamp. Centrifugation was performed on an Eppendorf 5417R Centrifuge. Absorbance was measured in a microplate reader (Synergy 2, Biotek, U.S.A.) in the MTT assay. The fluorescence images of the cells were taken by using a confocal laser scanning microscope (TCS SP8, Leica, Germany) with an objective lens (63×) and an excitation wavelength of 488 nm (10 mW). Imaging flow cytometry was accomplished on an Amnis ImageStream MarkII (Merck Millipore).

Synthesis of the Au NPs. The 13 nm Au NPs were prepared by the classical sodium citrate reduction method.[40] All glassware was cleaned in aqua regia (HCl/HNO_3, 3:1), washed triply with distilled H_2O, and oven-dried before the experiments. Typically, 70 mL of aqueous $HAuCl_4$ (0.01%) was heated to boiling under vigorous stirring, and then, trisodium citrate solution (3.5 mL, 1%) was added under stirring. The color of the solution first turned from pale yellow to colorless and eventually to burgundy. The solution was kept boiling for an additional 20 min. After the heating was stopped, the colloid was stirred until the prepared solution cooled to room temperature. Afterward, the solution was filtered through a 0.45 μm Millipore membrane filter. TEM images indicated the NPs are 13 ± 2 nm in average size. The prepared Au NPs were stored at 4 °C for future use.

Nanoprobe Synthesis. Sodium dodecyl sulfate solution (10%) was added to the Au NP solution (3 nM) to achieve a final concentration of 0.1%. The mixture was shaken for about 30 min, and then, selenol and thiol-modified peptide chains with FITC were added into the mixture (1 nM) with different concentrations (150, 300, 360, 450, 600, and 900 nM), respectively. The mixture under mildly shaking was saved in the dark for 48 h to complete the synthesis of the Au−Se probe and the Au−S probe. The nanoprobe solution was centrifuged (14 000 rpm, 25 min, 4 °C) and resuspended in Tris buffer solution (pH 7.4) three times. Consequently, the nanoprobe was resuspended in Tris buffer as stock solution and kept at 4 °C. The concentration of the Au NPs was calculated by the intensity of their extinction wavelength at 524 nm ($\varepsilon = 2.7 \times 10^8$ L mol^{-1} cm^{-1}).

Evaluation of NPs' Peptide Loading. The amount of each peptide loaded on the Au NPs was determined through a previously reported protocol with further modification.[41] Generally, mercaptoethanol was added (final concentration = 20 mM, 80 mM) to the nanoprobe (1 nM), and the mixture was stirred overnight at room temperature in the dark. Afterward, the released peptides were collected via centrifugation, and the fluorescence intensity of the supernatant solution was measured with a fluorescence spectrometer. For the FITC-labeled peptides, the fluorescence intensity was obtained at 490 nm excitation and 520 nm emission and converted to molar concentrations of the peptides by interpolation from a standard linear calibration curve that was prepared with known concentrations of peptide with identical buffer pH, mercaptoethanol concentration, and ionic strength. By dividing the molar concentrations of each peptide by the original concentration of the nanoprobes, the amount of peptides per nanoprobe was determined. All experiments were performed at least three times to check reproducibility.

Thermal Stability of the Two Nanoprobes. To test the temperature influence on the Au−Se probe and the Au−S probe, the two probes (1 nM) were incubated with increasing temperature (20, 30, 40, 50, 60, 70, 80 °C) for 5 min, respectively. Another test for the influence of time on the background fluorescence signals of the Au−Se probe and the Au−S probe was performed by incubating with an increasing time (0, 2, 4, 6, 8, 10, 12 h) at 37 °C, respectively. The fluorescence intensities of FITC were obtained with excitation/emission wavelengths at 490/520 nm. All experiments were performed at least three times.

GSH Effects on the Two Nanoprobes. The influence of GSH on the Au−Se probe and the Au−S probe was investigated by applying one group of the two different nanoprobes (1 nM), incubating each with 5 mM GSH for increasing times (0, 2, 4, 6, 8, 10, 12 h) at 37 °C and keeping the other group of the two nanoprobes samples each without GSH treatment to serve as control. In addition, the two nanoprobes (1 nM) were incubated with MMP-2 (10^{-1} μg/mL) at 37 °C, respectively, in the presence of 5 mM GSH. The fluorescence intensities of FITC were obtained with excitation/emission wavelengths at 490/520 nm. All experiments were performed at least three times.

Selenol Effects on the Au−Se Nanoprobe. The interference experiment of selenol to the Au−Se probe was performed. The levels of plasma selenium produced by normal dietary intake is about 120−134 g/L.[42] If all the selenium metabolized to selenol, the maximum concentration of selenol can raise up to 1.7 μM. Since selenocysteine (Sec) is one of the

DOI: 10.1021/acs.analchem.7b05343
Anal. Chem. 2018, 90, 4719−4724

most important metabolites of selenium,[43] 1.7 μM Sec was chosen to investigate the stability of the Au−Se probe against selenol. Sec was prepared following previous literature.[44] The Au−Se nanoprobe (1 nM) was incubated with MMP-2 (0.1 μg/mL) at 37 °C, in the absence and presence of 1.7 μM Sec for 30 min, respectively. The fluorescence intensities of FITC were obtained with excitation/emission wavelengths at 490/520 nm. All experiments were performed at least three times.

General Procedure for Fluorescence Determination. For analyte detection, the Au−Se probe and the Au−S probe (1 nM) was incubated with MMP-2 with increasing concentrations (10^{-7}, 10^{-6}, 10^{-5}, 10^{-4}, 10^{-3}, 10^{-2}, 10^{-1} μg/mL) for 0.5 h at 37 °C, respectively, in the presence of 5 mM GSH. For pH influence, the Au−Se probe (1 nM) was incubated with MMP-2 at 37 °C with the pH value ranging from 6.2 to 8.0. In the experiments for MMP-2 inhibition, one group of samples was treated with Marimastat, an MMP inhibitor, for 12 h, while another group of samples was not treated and served as the control group. The fluorescence intensities of FITC were obtained with excitation/emission wavelengths at 490/520 nm, and the experiments were finished at least three times.

Kinetics Study. The Au−Se probe (1 nM) was incubated with MMP-2 (0.1 μg/mL) at 37 °C. Then, the fluorescence intensities were determined on a certain time interval (0, 2.5, 5, 10, 15, 20, 25, 30, 35 min). The fluorescence intensities of FITC were obtained via excitation/emission wavelengths at 490/520 nm. The experiments were performed three times.

Biothiol Effects on the Two Nanoprobes. For the influence of biothiols on the Au−Se probe and the Au−S probe in vivo, HepG2 cells were plated on chamber slides for 24 h at first. One group of HepG2 cells was incubated with 500 μM *N*-ethylmaleimide for 20 min at 37 °C, and the other group of the samples was not treated and served as the control group. The two nanoprobes (1 nM) were respectively delivered HepG2 cells in DMEM culture medium at 37 °C in 5% CO_2 for 4 h. Then, the medium was removed, and the cells were washed three times with PBS and digested by trypsin and collected by centrifugation at 1000 rpm for 3 min. The bottom cells were washed twice with PBS, and the suspended cells were filtrated and examined by flow cytometry. The image and data of flow cytometer analysis were captured by fluorescence of FITC.

Confocal Fluorescence Image Assay. In a comparative experiment of cancer cells and normal cells, all cells were plated on chamber slides for 24 h. Then, the Au−Se probe (1 nM) was respectively delivered into MCF-7, HepG2, and HL-7702 cells in DMEM culture medium at 37 °C in 5% CO_2 for 4 h. Next, the cells were incubated with DAPI for 5 min and examined by a confocal laser scanning microscope with different laser transmitters. In the experiments for inhibiting MMP-2, one group of MCF-7 cells and HepG2 cells was treated with Marimastat for 12 h, and another group of cells was not treated and served as the control group. The same steps were performed using the Au−Se probe (1 nM) instead. Finally, the cells were imaged by a confocal laser scanning microscope. All experiments were performed at least three times.

RESULTS AND DISCUSSION

Preparation and Characterization of the Nanoprobes. First, the Au NPs were synthesized according to a reported method with certain modifications.[40] To prepare the two different nanoprobes (Au−Se probe and Au−S probe), the Au NPs were functionalized with selenol-modified and thiol-modified peptides via Au−Se bond and Au−S bond formation (Figure 1a). As shown in Figures 1 and S5, compared to the

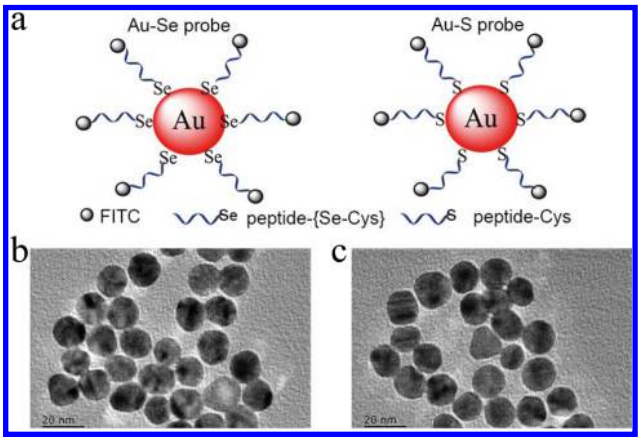

Figure 1. (a) Schematic illustration of the design of the Au−Se nanoprobe and the Au−S nanoprobe. TEM image of (b) the Au−Se nanoprobes and (c) the Au−S nanoprobes. Scale bars are 20 nm.

bare Au NPs, the morphology of the two nanoprobes did not show significant changes, and the average diameters of the two nanoprobes were close to about 13 nm. The UV−vis absorption spectra displayed that the maximum absorption peak of the bare Au NPs was 520 nm while that of the two nanoprobes was 524 nm, which had resulted from the functionalization of peptides on the surface of the Au NPs (Figure S6). Then, the quantification of the peptides on the Au NPs were carried by using a fluorescence-based method according to a previous protocol[41] with further modification (Figure S7). Table S1 shows that under the same conditions, each Au NP carries more selenol-modified peptides compared to thiol-modified peptides. It is obvious that during the nanoprobe synthesis, the Au−Se bond forms more easily than the Au−S bond. To ensure the accuracy of the experimental conditions, the number of replaced peptides for each Au NP was chosen to be ∼47 for the Au−Se probe and ∼48 for the Au−S probe.

Thermal Stability of the Two Nanoprobes. As shown in Figure S8, the excitation wavelength and emission wavelength of the two nanoprobes are 490/520 nm, indicating that Se and S do not influence the probes' spectral properties. For further investigation of the thermal stability, the two nanoprobes (1 nM) were incubated respectively with increasing temperature. The background fluorescence signal of the Au−Se probe exhibits almost no change, whereas the signal of the Au−S probe gradually increases with the rise of the temperature due to rupturing of the Au−S bond (Figure 2a), demonstrating a high thermal stability of the Au−Se probe. Subsequently, to study the time influence, the two different nanoprobes (1 nM) were incubated respectively for various times at 37 °C. The background fluorescence signal of the Au−Se probe remained basically unchanged, while the Au−S probe has obvious signal enhancement (Figure 2b), which further proves that the Au−Se probe owns better stability.

Effects of GSH on the Two Nanoprobes. To manifest the anti-interference characteristic of the Au−Se probe in vitro, the reciprocity of the two nanoprobes with GSH was then investigated. One group of the two nanoprobes (1 nM) was incubated separately with GSH at 37 °C for different times, respectively. The other group of the two nanoprobe samples

DOI: 10.1021/acs.analchem.7b05343
Anal. Chem. 2018, 90, 4719−4724

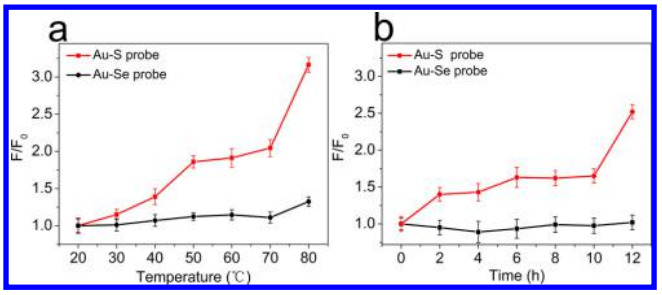

Figure 2. (a) Temperature effects and (b) time effects at 37 °C on the background fluorescence signals of the two different nanoprobes.

without any treatment served as the control group. In Figure 3a, after addition of GSH to the Au−Se probe solutions, the

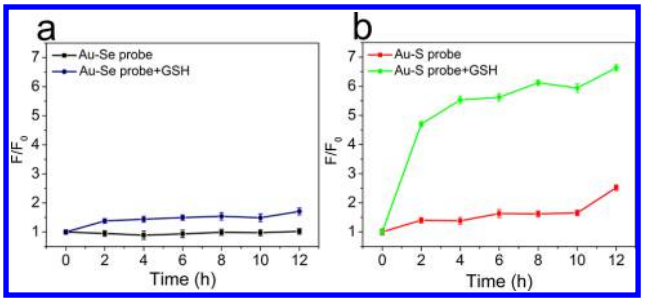

Figure 3. GSH effects (5 mM)on the background fluorescence signals of (a) the Au−Se nanoprobe (1 nM) and (b) the Au−S nanoprobe (1 nM).

fluorescence intensity did not exhibit any obvious change. However, the Au−S probe displayed sharply increased signal intensity with the presence of GSH (Figure 3b). This phenomenon is due to interruption of GSH on the Au−S bond, resulting in erroneous signal changes. However, with the Au−Se bond's higher stability, the Au−Se probe possesses an anti-interference characteristic.

Moreover, the two nanoprobes (1 nM) were incubated with MMP-2 with increasing concentrations at 37 °C, in the presence of 5 mM GSH. The Au−Se probe shows a significantly enhanced fluorescence signal as compared to the Au−S probe's response to MMP-2 when GSH was added to the solutions (Figure 4). It can be calculated that the Au−Se probe possesses a high SNR (10.1) and a low LOD (1.7 ng/mL) under simulated physiological conditions, better than the Au−S probe's SNR (3.9) and LOD (3.1 ng/mL). It can be revealed that the Au−Se probe could avoid the false positive results that

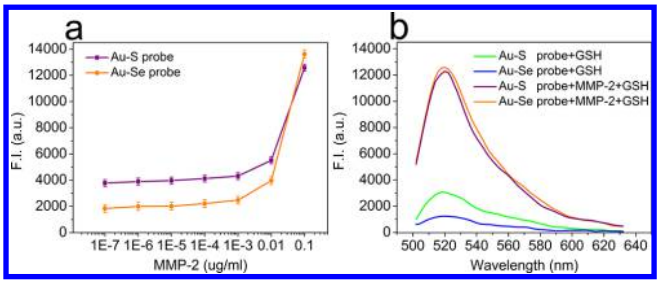

Figure 4. (a) GSH effects (5 mM) on fluorescence signals in the process of two probes' (1 nM) response to MMP-2. (b) GSH effects (5 mM) on the background fluorescence signals of the two probes (1 nM), in the presence of 0.1 μg/mL MMP-2.

were produced by Au−S bond breaking, and it has an outstanding anti-interference characteristic. As shown in Figure S9, the fluorescence intensities of the Au−Se probes' responses to MMP-2 both increased about 9.6-fold in the absence and presence of 1.7 μM Sec, which demonstrated that the Au−Se probe owns high resistance toward a physiological level of selenol. This is especially important for the nanoprobes to achieve intracellular detection of molecules in physiological environments.

Cytotoxicity Assay. To evaluate the cytotoxicity, the MTT assay in human liver cancer cell line HepG2 was performed. Since the absorbance of MTT at 490 nm is dependent upon the degree of activation of the cells, the Au NPs and the two probes (1 nM) had no obvious effect on HepG2 cell viability for times up to 24 h (Figure S10). Therefore, it suggests that the probe exhibits low biotoxicity or side effects in living cells and could be applied for detecting MMP-2 in biological samples.

Intracellular Biothiol Effects. To further verify the anti-interference performance of the Au−Se probe in vivo, flow cytometry was performed for the nanoprobes in HepG2 cell lines. One group of HepG2 cells was incubated with 500 μM *N*-ethylmaleimide for 20 min at 37 °C, and the other group of the cells without any treatment served as the control group. The two probes (1 nM) were respectively delivered HepG2 cells in DMEM culture medium at 37 °C in 5% CO_2 for 4 h. In Figure 5, the response of the Au−Se probe and the Au−S probe to

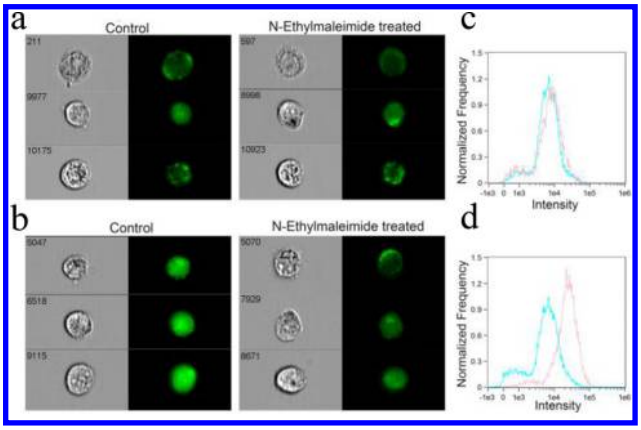

Figure 5. Flow cytometry imaging of biothiol effects on (a) the Au−Se probe and (b) the Au−S probe in HepG2 cells. (c,d) The flow cytometry data analysis of the fluorescence intensity of cells was consistent with the above results (a,b).

MMP-2 was compared to represent the peptide cleavage abilities. There is no change in fluorescence intensity for the comparison of the Au−Se probe incubated with and without *N*-ethylmaleimide (Figure 5a). In contrast, a gradually increasing false positive signal of the Au−S probe was obtained both before and after eliminating biothiols with *N*-ethylmaleimide (Figure 5b). The flow cytometry analysis of fluorescence intensity of the cells was consistent with the above results (Figure 5c,d), further revealing that the Au−Se probe can avoid the detection signal distortion caused by biothiols. The Au−Se probe possesses excellent stability and a strong anti-interference property, which makes it a more accurately reliable probe for MMP-2-targeted detection in cancer diagnosis.

Fluorescence Determination in Vitro. In order to test the Au−Se probe detection toward MMP-2 changes, one group of the samples was treated with Marimastat for 12 h, and

DOI: 10.1021/acs.analchem.7b05343
Anal. Chem. 2018, 90, 4719−4724

another group was set as the control group without any treatment. Notably, the reaction can be terminated by Marimastat, the inhibitor of MMP-2, which was observed from the decrease in fluorescence intensity in Figure S11. In addition, as the response time to target intracellular MMP-2 is also a critical property for the probes, the release rate of FITC was investigated. An excess of target, MMP-2 was added to the Au−Se probe solution, and the fluorescence intensity change over time was monitored. Figure 6a shows that fluorescence of

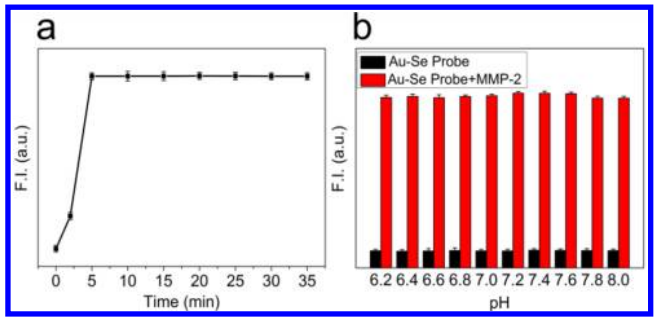

Figure 6. (a) Kinetics of the Au−Se probe. The nanoprobe (1 nM) was incubated with MMP-2, and the MMP-2 activities are 0.1 μg/mL. (b) Fluorescence intensity changes of the Au−Se probe (1 nM) at different pH values in the absence (black bars) or presence (red bars) of MMP-2 (0.1 μg/mL). Data are shown as mean ± SD of three independent experiments performed in duplicate.

FITC first increases rapidly, reaching completion in ~30 min, which compares favorably to the Au−S probe. Furthermore, the fluorescence intensity of the Au−Se probe did not change significantly in different pHs (Figure 6b), demonstrating that the designed Au−Se probe was able to monitor MMP-2 fluctuation without interference.

Au−Se Probe with MMP-2 in Vivo. In order to further examine the validity of the Au−Se probe for intracellular MMP-2 detection, the HepG2 cell and MCF-7 cell, where MMP-2 was overexpressed, were chosen. These cells were incubated with the Au−Se probe (1 nM) at 37 °C for about 4 h and then were incubated with DAPI for 5 min. As shown in Figure 7a, for

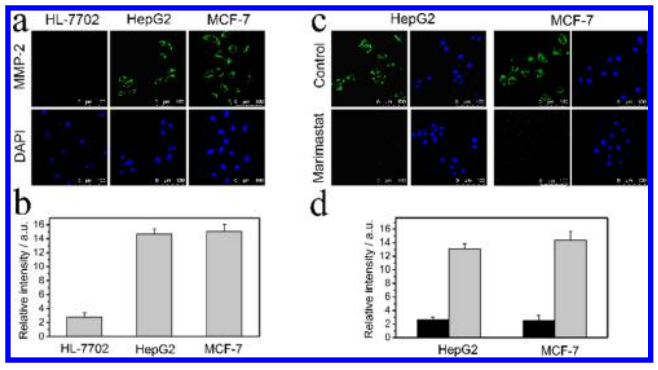

Figure 7. (a) Fluorescence images of intracellular MMP-2 and nucleus staining images in HL-7702, HepG2, and MCF-7 cells by the Au−Se probe with confocal laser scanning microscope. (b) Relative fluorescence intensity of the above three cell lines. (c) Fluorescence images of MMP-2 and nucleus staining images in HepG2 cells and MCF-7 cells treated without and with Marimastat by the Au−Se probe (1 nM). (d) Relative fluorescence intensity from MMP-2 of the above two cell lines. Nuclei were stained with DAPI (blue). Scale bars are 100 μm (λ_{em} = 500−560 nm). Data are shown as mean ± SD of three independent experiments performed in duplicate.

the HepG2 cell and MCF-7 cell, the fluorescence intensity of the Au−Se probe was significantly enhanced due to the hybridization of the nanoprobe and peptide targets, which leads to fluorescence recovery, indicating that MMP-2 specifically cleaved the substrate peptide and efficiently released FITC from the Au NPs. Simultaneously, there is no fluorescence signal in normal HL-7702 cells. Also, the Au−Se probes' detection of the changes of MMP expression levels in living cells was also considered. The result is consistent with the in vitro experiment, which also means that the reaction can be terminated by the inhibitor of MMP-2, showing a decrease in fluorescence intensity (Figure 7c). In Figure 7b,d, the quantification of fluorescence intensity indicated that the designed nanoprobe was able to monitor MMP-2 fluctuation and reflects the true level of intracellular MMP-2.

CONCLUSIONS

In summary, a new type of nanoprobe based on the Au−Se bond was designed and synthesized. The probe can be successfully applied to high-fidelity imaging of MMP-2 in HepG2 cells and MCF-7 cells. In comparison to the previously reported Au−S probe, the Au−Se probe displayed a higher SNR (10.1) and a lower LOD (1.7 ng/mL) under simulated physiological conditions. The Au−Se probe shows high thermal stability and immunity to interference. More importantly, the Au−Se probe can avoid interference caused by high levels of in vivo thiol compounds and provide actual information on target molecules in biological systems. The fluorescence intensity signals from the tumor cells treated with the probe have barely changed in the presence and elimination of GSH. We foresee that the Au−Se bond strategy has exciting potential applications to create a variety of new sensors for the detection of other important intracellular biomolecules under high concentrations of biothiols.

ASSOCIATED CONTENT

Supporting Information

The Supporting Information is available free of charge via the Internet at The Supporting Information is available free of charge on the ACS Publications website at DOI: 10.1021/acs.analchem.7b05343.

Experimental procedures and additional data (PDF)

AUTHOR INFORMATION

Corresponding Authors

*E-mail: xukehua@sdnu.edu.cn (K.X.)
*E-mail: tangb@sdnu.edu.cn (B.T.)

ORCID

Bo Tang: 0000-0002-8712-7025

Author Contributions

†X.G. and L.J. contributed equally to this work.

Notes

The authors declare no competing financial interest.

ACKNOWLEDGMENTS

This work was supported by the National Natural Science Foundation of China (21535004, 91753111, 21390411, 21575081, 21775091, and 21705098).

DOI: 10.1021/acs.analchem.7b05343
Anal. Chem. 2018, 90, 4719−4724

REFERENCES

(1) Zheng, T.; Pierre-Pierre, N.; Yan, X.; Huo, Q.; Almodovar, A. J. O.; Valerio, F.; Rivera-Ramirez, I.; Griffith, E.; Decker, D. D.; Chen, S.; Zhu, N. *ACS Appl. Mater. Interfaces* **2015**, *7*, 6819−6827.
(2) Yu, Y.; Wu, Y.; Liu, J.; Li, K.; Wu, D. *J. Mater. Chem. B* **2016**, *4*, 1090−1099.
(3) Primo, A.; Corma, A.; García, H. *Phys. Chem. Chem. Phys.* **2011**, *13*, 886−910.
(4) Liu, J.; Zhang, L.; Lei, J.; Ju, H. *ACS Appl. Mater. Interfaces* **2015**, *7*, 19016−19023.
(5) He, W.; Ai, K.; Jiang, C.; Li, Y.; Song, X.; Lu, L. *Biomaterials* **2017**, *132*, 37−47.
(6) Jiang, H.; Chen, D.; Guo, D.; Wang, N.; Su, Y.; Jin, X.; Tong, G.; Zhu, X. *Biomater. Sci.* **2017**, *5*, 686−697.
(7) Morgan, F.; Murphy, A.; Hendren, W.; Wurtz, G.; Pollard, R. J. *ACS Appl. Mater. Interfaces* **2017**, *9*, 17379−17386.
(8) Mirkin, C. A.; Letsinger, R. L.; Mucic, R. C.; Storhoff, J. J. *Nature* **1996**, *382*, 607−609.
(9) Alivisatos, A. P.; Johnsson, K. P.; Peng, X.; Wilson, T. E.; Loweth, C. J.; Bruchez, M. P., Jr; Schultz, P. G. *Nature* **1996**, *382*, 609−611.
(10) Ramya, A. N.; Joseph, M. M.; Nair, J. B.; Karunakaran, V.; Narayanan, N.; Maiti, K. K. *ACS Appl. Mater. Interfaces* **2016**, *8*, 10220−10225.
(11) Shangguan, J.; Huang, J.; He, D.; He, X.; Wang, K.; Ye, R.; Yang, X.; Qing, T.; Tang, J. *Anal. Chem.* **2017**, *89*, 7477−7484.
(12) Wang, W.; Zhang, L.; Li, L.; Tian, Y. *Anal. Chem.* **2016**, *88*, 9518−9523.
(13) Wang, X.; Qian, X.; Beitler, J. J.; Chen, Z. G.; Khuri, F. R.; Lewis, M. M.; Shin, H. J. C.; Nie, S.; Shin, D. M. *Cancer Res.* **2011**, *71*, 1526−1532.
(14) Luan, M.; Li, N.; Pan, W.; Yang, L.; Yu, Z.; Tang, B. *Chem. Commun.* **2017**, *53*, 356−359.
(15) Yang, L.; Chen, Y.; Pan, W.; Wang, H.; Li, N.; Tang, B. *Anal. Chem.* **2017**, *89*, 6196−6201.
(16) He, G.; Li, J.; Wang, Z.; Liu, C.; Liu, X.; Ji, L.; Xie, C.; Wang, Q. *Tetrahedron* **2017**, *73*, 272−277.
(17) Aravanis, A. M.; Lee, M.; Klausner, R. D. *Cell* **2017**, *168*, 571−574.
(18) Yang, Y.; Huang, J.; Yang, X.; Quan, K.; Wang, H.; Ying, L.; Xie, N.; Ou, M.; Wang, K. *J. Am. Chem. Soc.* **2015**, *137*, 8340−8343.
(19) Pan, W.; Yang, H.; Li, N.; Yang, L.; Tang, B. *Chem. - Eur. J.* **2015**, *21*, 6070−6073.
(20) Hu, B.; Cheng, R.; Liu, X.; Pan, X.; Kong, F.; Gao, W.; Xu, K.; Tang, B. *Biomaterials* **2016**, *92*, 81−89.
(21) Liu, X.; Hu, B.; Cheng, R.; Kong, F.; Pan, X.; Xu, K.; Tang, B. *Chem. Commun.* **2016**, *52*, 6693−6696.
(22) Golzhauser, A.; Woll, C. *ChemPhysChem* **2010**, *11*, 3201−3213.
(23) Hohman, J. N.; Thomas, J. C.; Zhao, Y.; Auluck, H.; Kim, M.; Vijselaar, W.; Kommeren, S.; Terfort, A.; Weiss, P. S. *J. Am. Chem. Soc.* **2014**, *136*, 8110−8121.
(24) Jackson-Rosario, S.; Cowart, D.; Myers, A.; Tarrien, R.; Levine, R. L.; Scott, R. A.; Self, W. T. *JBIC, J. Biol. Inorg. Chem.* **2009**, *14*, 507−519.
(25) Othman, H.; Wieninger, S. A.; ElAyeb, M.; Nilges, M.; Srairi-Abid, N. *J. Biomol. Struct. Dyn.* **2017**, *35*, 2815−2829.
(26) Zhang, M.; Hu, X.; Li, S.; Lu, C.; Li, J.; Zong, Y.; Qi, W.; Yang, H. *Clin. Res. Hepatol. Gastroenterol.* **2018**, *42*, 72.
(27) Isaacson, K. J.; Martin Jensen, M.; Subrahmanyam, N. B.; Ghandehari, H. *J. Controlled Release* **2017**, *259*, 62−75.
(28) Bourboulia, D.; Stetler-Stevenson, W. G. *Semin. Cancer Biol.* **2010**, *20*, 161−168.
(29) Lukaszewicz-Zajac, M.; Mroczko, B.; Szmitkowski, M. *Clin. Chim. Acta* **2011**, *412*, 1725−1730.
(30) Gao, H.; Dang, Q.; Xia, S.; Zhao, Y.; Qi, H.; Gao, Q.; Zhang, C. *Sens. Actuators, B* **2017**, *253*, 69−76.
(31) Araújo, R. F., Jr; Lira, G. A.; Vilaça, J. A.; Guedes, H. G.; Leitão, M. C. A.; Lucena, H. F.; Ramos, C. C. O. *Pathol., Res. Pract.* **2015**, *211*, 71−77.
(32) Li, J.; Zeng, Q.; Zhang, Y.; Li, X.; Hu, H.; Miao, X.; Yang, W.; Zhang, W.; Song, X.; Mou, L.; Wang, R. *Eur. J. Cell Biol.* **2016**, *95*, 368−377.
(33) Chowdhury, A.; Nandy, S. K.; Sarkar, J.; Chakraborti, T.; Chakraborti, S. *Mol. Cell. Biochem.* **2017**, *427*, 111−122.
(34) Sun, J.; Luo, Q.; Liu, L.; Yang, X.; Zhu, S.; Song, G. *Toxicology* **2017**, *384*, 1−10.
(35) Affo, S.; Yu, L. X.; Schwabe, R. F. *Annu. Rev. Pathol.: Mech. Dis.* **2017**, *12*, 153−186.
(36) Bautista-Lopez, B.; Galipeau, J.; Cuerquis, J.; Lalu, M. M.; Eliopoulos, N. *J. Clin Exp Oncol* **2017**, *06*, 2.
(37) Xie, G.; Wang, Z.; Chen, Y.; Zhang, S.; Feng, L.; Meng, F.; Yu, Z. *Cancer Lett.* **2017**, *388*, 12−20.
(38) Yin, Z.; Sun, Y.; Ge, S.; Sun, J. *Oncol. Rep.* **2017**, *37*, 2286−2294.
(39) Oriana, S.; Cai, Y.; Bode, J. W.; Yamakoshi, Y. *Org. Biomol. Chem.* **2017**, *15*, 1792−1800.
(40) Jiang, Y.; Shi, M.; Liu, Y.; Wan, S.; Cui, C.; Zhang, L.; Tan, W. *Angew. Chem., Int. Ed.* **2017**, *56*, 11916−11920.
(41) Luan, M.; Yu, L.; Li, Y.; Pan, W.; Gao, X.; Wan, X.; Li, N.; Tang, B. *Anal. Chem.* **2017**, *89*, 10601−10607.
(42) Rayman, M. P. *Lancet* **2000**, *356*, 233−241.
(43) Roman, M.; Jitaru, P.; Barbante, C. *Metallomics* **2014**, *6*, 25−54.
(44) Kong, F.; Hu, B.; Gao, Y.; Xu, K.; Pan, X.; Huang, F.; Zheng, Q.; Chen, H.; Tang, B. *Chem. Commun.* **2015**, *51*, 3102−3105.

DOI: 10.1021/acs.analchem.7b05343
Anal. Chem. 2018, 90, 4719−4724